Electronic Supplementary Information (ESI)

Improving the Performance of QSEDLCs by Modulating the Properties of Electrolytes from Bulk to Interfaces

Siyuan Xu and Guangming Liu*

Department of Chemical Physics, Key Laboratory of Surface and Interface Chemistry and Energy Catalysis of Anhui Higher Education Institutes, University of Science and Technology of China, Hefei, P. R. China 230026

*Corresponding Author: gml@ustc.edu.cn (Email).

Materials and methods

Materials. Propylsulfonate dimethylammonium propylmethacrylamide (PDP) (≥ 98%, Changzhou YiPinTang Chemical Co. Ltd.), *N,N*′-methylenebisacrylamide (MBAA) (99.5%, Aladdin), ammonium persulfate (APS) ($(NH_4)_2S_2O_8$, 98%, Sinopharm), lithium perchlorate ($LiClO_4$, 99.99%, Aladdin), sodium perchlorate ($NaClO_4$, 99.99%, Aladdin), poly(vinyl alcohol) (PVA, molecular weight ~ 7.5×10^4 g mol^{-1}, Sinopharm), propene carbonate (PC, 99.0%, Aladdin), formamide (FA, 99.5%, Sinopharm), acetonitrile (ACN, 99.5%, Sinopharm), dimethyl sulfoxide (DMSO, 99.5%, Sinopharm), YP-50F activated carbon (Kuraray Co.), polytetrafluoroethylene (PTFE) emulsion (60 wt% in H_2O, Daikin Industries, Ltd.), and acetylene black (MTI Company) were all used as received.

Preparation of gel electrolytes. The PPDP-Li^+/Na^+ was prepared as follows. 0.75 g PDP, 30.0 mg MBAA, and 27.0 mg $(NH_4)_2S_2O_8$ were dissolved in water (1.125 g) in a glass vial with a nitrogen bubbling for a certain time at room temperature. Afterward, 1.0 g $NaClO_4$ and 1.5 g $LiClO_4$ were successively added in the glass vial at room temperature, followed by a shaking of the glass vial during the heating with a water bath at ~ 80 °C to facilitate a complete dissolution and a homogeneous distribution of $NaClO_4$ and $LiClO_4$ until a homogeneous and transpararent sample was obtained. Then, the polymerization was performed in an oven at 80 °C for ~ 6 h. The PPDP-Li^+ (PPDP-Na^+) was prepared by a similar procedure in the absence of $NaClO_4$ ($LiClO_4$). The PVA-Li^+/Na^+ was prepared as follows. 0.75 g PVA was mixed with 6.75 g water, and then the mixture was heated and stirred for ~ 2 h at ~ 90 °C to obtain the PVA solution with

a concentration of 10 wt%. Afterwards, 1.5 g $LiClO_4$ and 1.0 g $NaClO_4$ were added to the PVA solution to obtain the PVA-Li^+/Na^+ through a solvent evaporation at ~ 80 °C until the water content reached 1.125 g.

Fabrication of electrodes and supercapacitors. It is known that the YP-50F activated carbon with the advantages of low cost and high specific surface area has been widely used to fabricate the electrodes for supercapacitors.[S1,S2] For the fabrication of electrodes in this work, the commercial YP-50F activated carbon powder, PTFE emulsion (10 wt% in H_2O), and conductive acetylene black with a mass ratio of 7:2:1 were mixed with a certain amount of ethanol to form a paste. The paste was sandwiched by two pieces of copper foil (thickness ~ 10 μm) and rolled by double-roller press at room temperature to prepare the electrodes with different thicknesses but the same density. Afterwards, the electrodes were dried at ~ 80 °C for ~ 10 h in a vacuum oven. For fabrication of the PPDP-Li^+/Na^+-PC- and PVA-Li^+/Na^+-PC-based QSEDLCs, the electrodes were immersed in a 2.8 M $LiClO_4$ PC solution for 40 min, and then the supercapacitors were assembled with a corresponding GPE and two pieces of electrodes inside a CR2032 coin cell.

Electrochemical tests. The electrochemical performances including cyclic voltammetry (CV), galvanostatic charge and discharge (GCD), electrochemical impedance spectroscopy (EIS), and self-discharge of the supercapacitors were measured using a Bio-logic VMP-300 electrochemical workstation. The EIS was

obtained under open circuit potential with an AC amplitude of 10 mV and a frequency range from 100 kHz to 100 mHz. In this work, the specific capacitance was calculated based on the mass of the active material of one electrode. The specific energy and specific power were calculated based on the mass of the active material of two electrodes. The voltage after *IR* drop and the discharge time were used to calculate the specific capacitance from the GCD curves.

Other characterizations.

The ionic conductivities of the GPEs were determined from the EIS measurements according to the previous studies.[S3-S5] The stress-strain curves for the cyclic compression and relaxation of the samples were measured by an electronic universal testing machine (TS7104, Shenzhen SANS Material Testing CO., LTD.) at a speed of 10 mm min^{-1} with the exception of Fig. S5c. The differential scanning calorimetry (DSC) tests were conducted with a heating rate of 5.0 °C min^{-1} (DSC Q2000, TA Instrument). The contact angles were determined using a contact angle goniometer (CAM 200, KSV) at ~ 25 °C. The UV/vis spectra were obtained using a UNICO 2802 UV/visible spectrophotometer at ~ 25 °C. The micromorphology of hydrogels was obtained using a confocal microscopy (Olympus IX81) at ~ 25 °C. The energy dispersive X-ray spectroscopy (EDS) measurements were conducted on a field emission scanning electron microscope (GeminiSEM 500). Raman spectroscopy measurements were conducted on a Raman Spectrometer (LabRamHR Evolution).

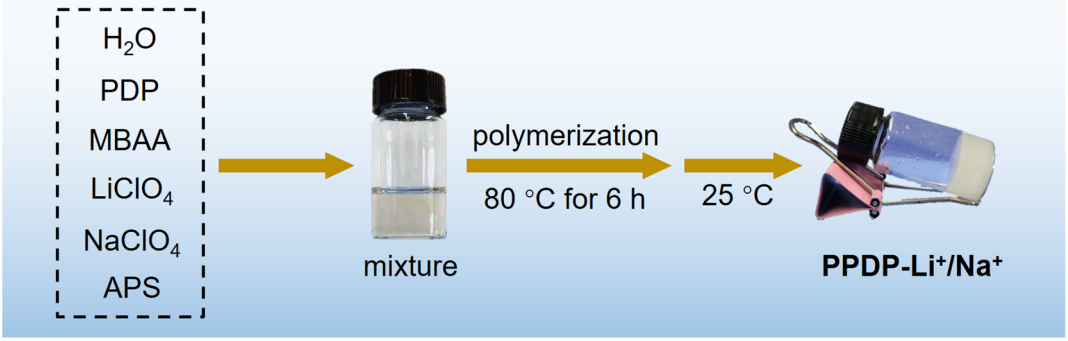

Fig. S1. Schematic illustration of the preparation of PPDP-Li^+/Na^+ through the polymerization of PPDP at ~ 80 °C in the presence of $LiClO_4$ and $NaClO_4$.

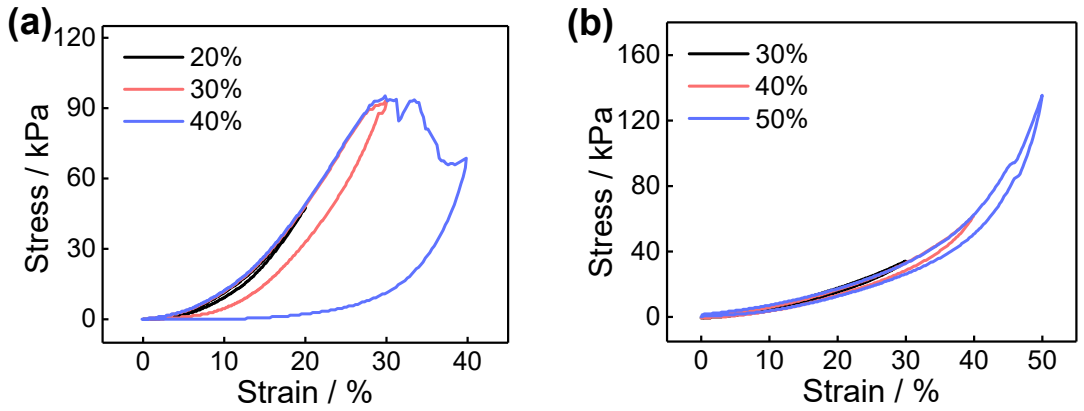

Fig. S2. The stress-strain curves for the cyclic compression and relaxation of the samples at different strains. (a) PPDP-H, and (b) PPDP-Li^+.

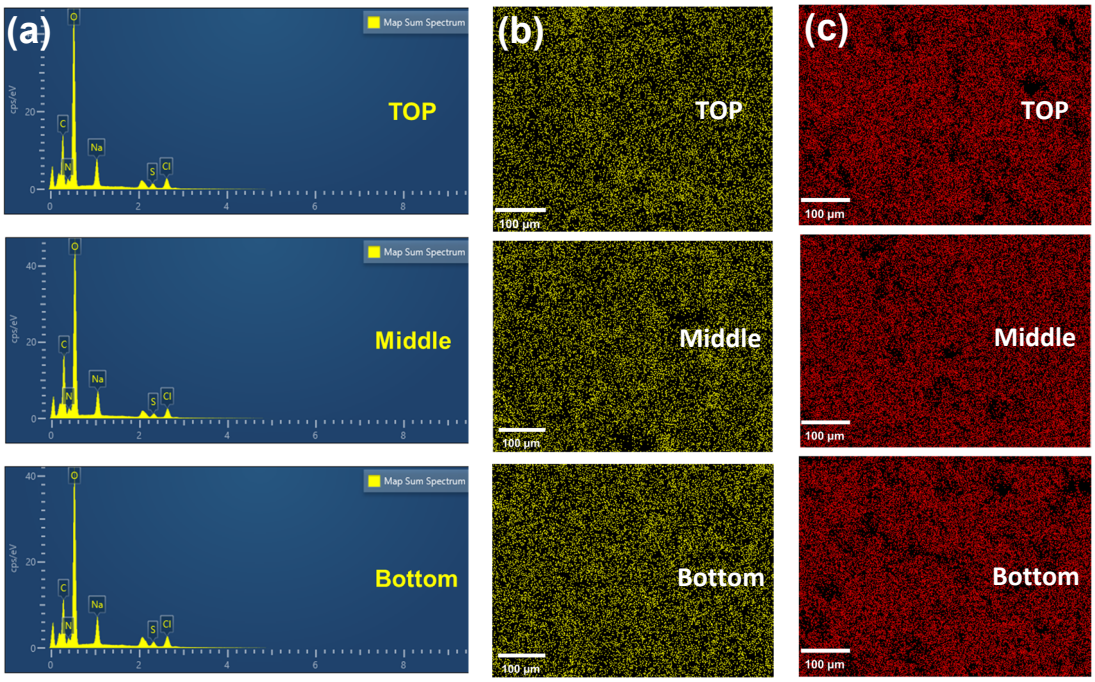

Fig. S3. The EDS measurements of the top, middle, and bottom parts of the PPDP-Li^+/Na^+ sample. (a) EDS spectra. (b) and (c) EDS elemental mapping images. (b) Cl, and (c) Na.

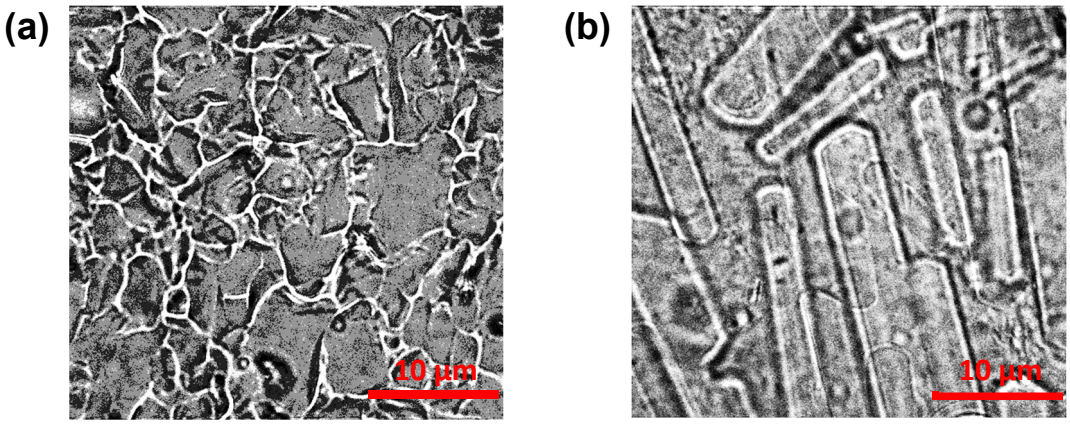

Fig. S4. The images of the samples obtained from the confocal microscopy. (a) PPDP-H, and (b) PPDP-Li^+/Na^+.

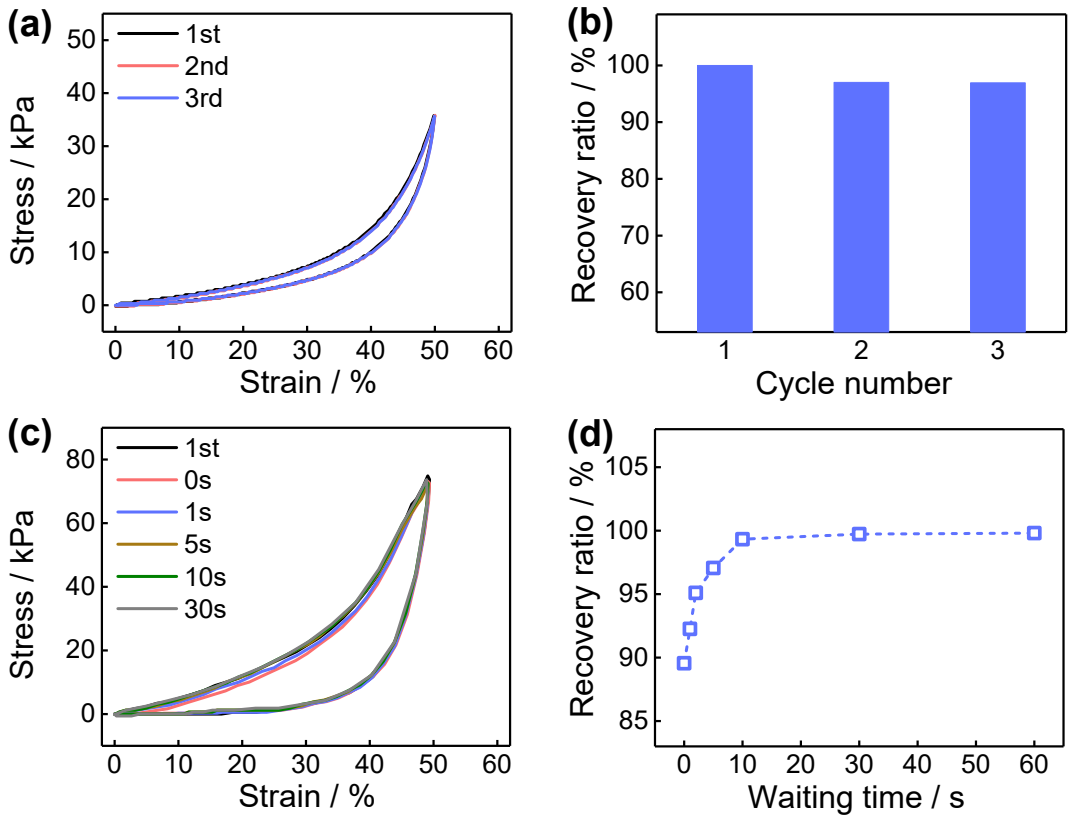

Fig. S5. (a) The stress-strain curves for the 1st, 2nd, and 3rd cycles of compression and relaxation of PPDP-Li^+/Na^+ at a strain of 50% with a speed of 10 mm min^{-1}. (b) The recovery ratio of the PPDP-Li^+/Na^+ sample as a function of cycle number of the cyclic compression and relaxation, calculated based on the areas under the stress-strain curves during the compression process in panel (a). (c) The stress-strain curves for the cyclic compression and relaxation of PPDP-Li^+/Na^+ at a strain of 50% with a speed of 300 mm min^{-1} as a function of waiting time at a strain of 0% following the 1st cycle of compression and relaxation. (d) The recovery ratio of the PPDP-Li^+/Na^+ sample as a function of waiting time at a strain of 0% following the 1st cycle of compression and relaxation, calculated based on the areas under the stress-strain curves during the compression process in panel (c).

The results in Fig. S5a and S5b indicate that the physical bonds which are broken in the compression process can almost recover during the relaxation process when the cyclic compression and relaxation of PPDP-Li^+/Na^+ is conducted with a speed of 10 mm min^{-1}. In order to quantitatively analyze the recovery rate, we have conducted the cyclic compression and relaxation of the PPDP-Li^+/Na^+ sample at a strain of 50% with a speed of 300 mm min^{-1} (Fig. S5c). The results indicate that the physical bonds which are broken during the compression process can recover completely after the waiting time of ~ 30 s at a strain of 0% following the 1st cycle of compression and relaxation (Fig. S5d).

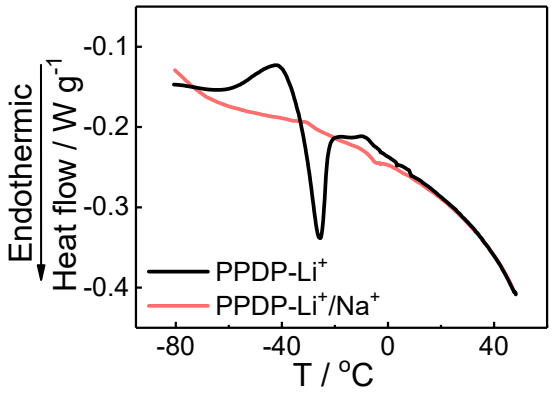

Fig. S6. DSC thermograms of PPDP-Li^+ and PPDP-Li^+/Na^+ in a temperature range from -80 to 50 °C.

In Fig. S6, an obvious endothermic peak is observed in the thermogram of PPDP-Li^+, indicating that freezable water can be detected in the PPDP-Li^+ sample. In contrast, no obvious endothermic peak can be observed in the thermogram of PPDP-Li^+/Na^+, suggesting that no freezable water can be detected in the PPDP-Li^+/Na^+ sample. This fact indicates that the water activity in the PPDP-Li^+/Na^+ sample is lower than that in the PPDP-Li^+ sample.

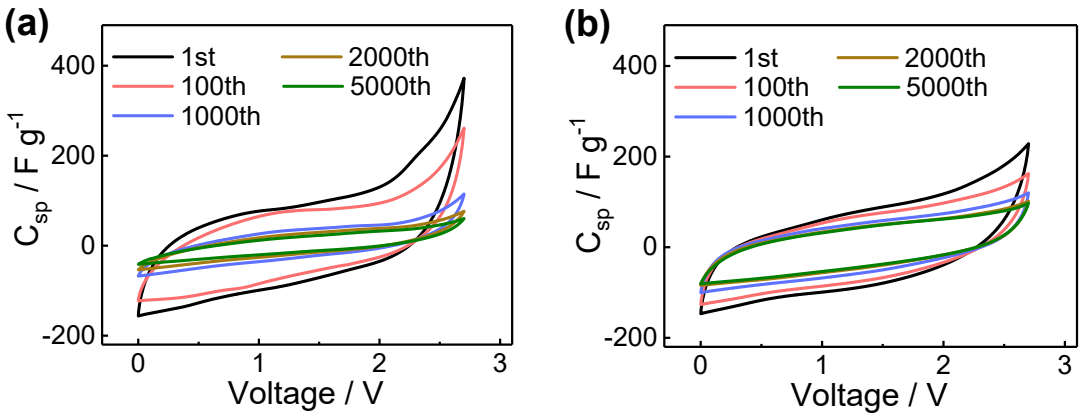

Fig. S7. CV curves of the supercapacitors as a function of cycle number at a scan rate of 100 mV s^{-1} in the range of voltage from 0 to 2.7 V. (a) PPDP-Li^+-based QSEDLC. (b) PPDP-Li^+/Na^+-based QSEDLC.

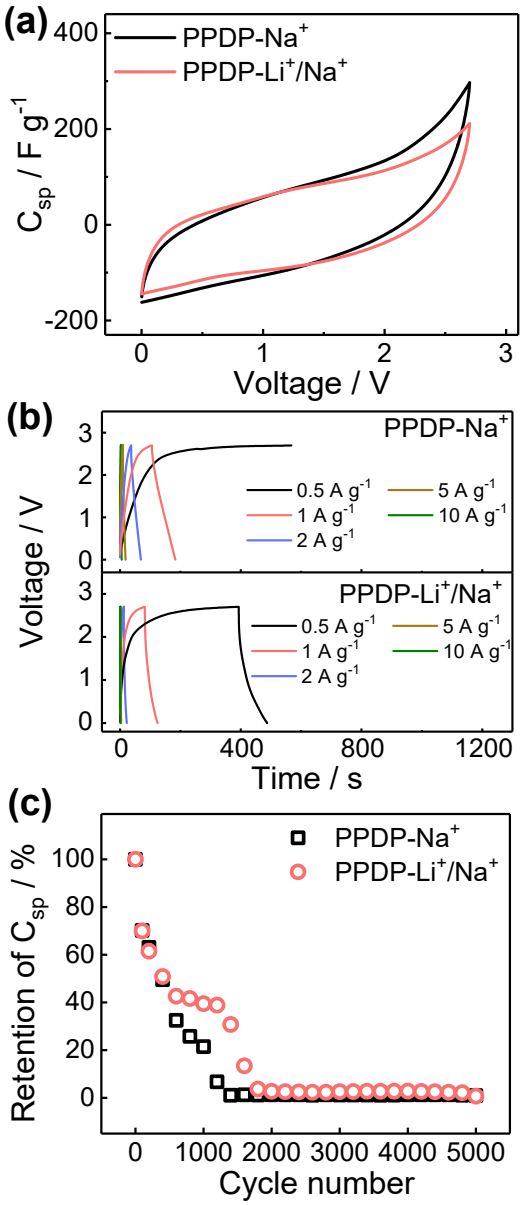

Fig. S8. Comparison of the electrochemical performances between PPDP-Na^+- and PPDP-Li^+/Na^+-based QSEDLCs in the range of voltage from 0 to 2.7 V. (a) CV curves at a scan rate of 100 mV s^{-1}. (b) GCD curves in the range of current density from 0.5 to 10 A g^{-1}. (c) Cycling performance at a current density of 1.0 A g^{-1}. Here, the PPDP-Na^+ is prepared by dissolving 3.75 g $NaClO_4$ in 1.125 g water.

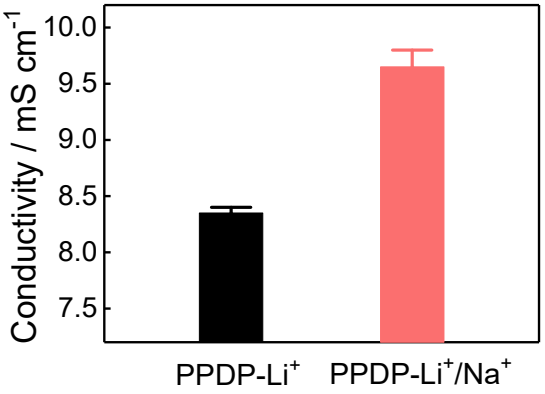

Fig. S9. The ionic conductivities of PPDP-Li^+ and PPDP-Li^+/Na^+ determined from the EIS measurements at ~ 25 °C.

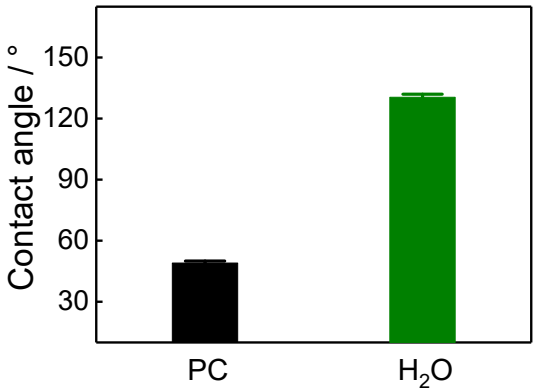

Fig. S10. Contact angles of PC and H_2O on the surface of the activated carbon electrode at ~ 25 °C.

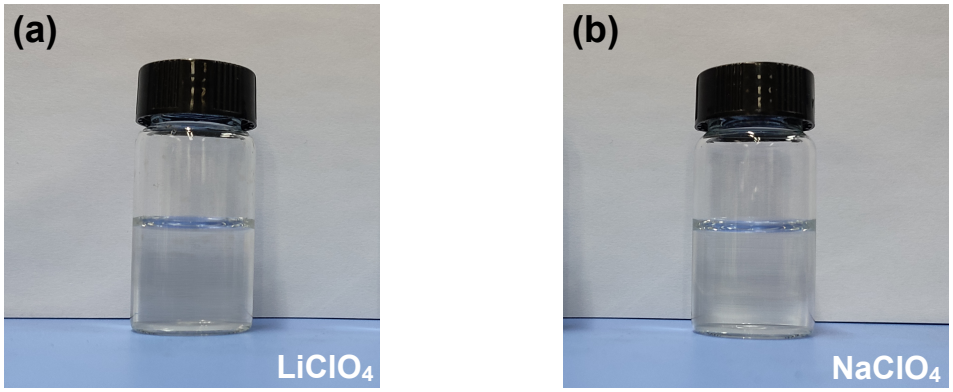

Fig. S11. The images of the PC electrolyte solutions. (a) 2.8 M $LiClO_4$, and (b) 2.0 M $NaClO_4$.

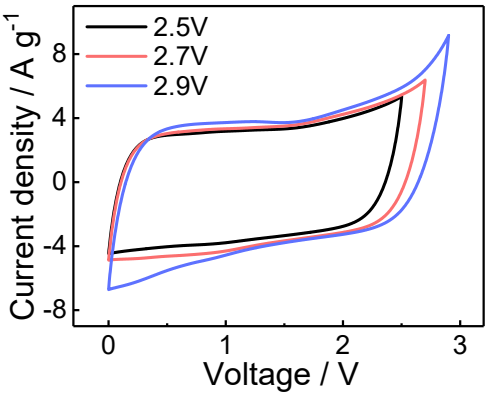

Fig. S12. CV curves for the PPDP-Li^+/Na^+-PC-based QSEDLC at a scan rate of 100 mV s^{-1} with different cut-off voltages from 2.5 to 2.9 V.

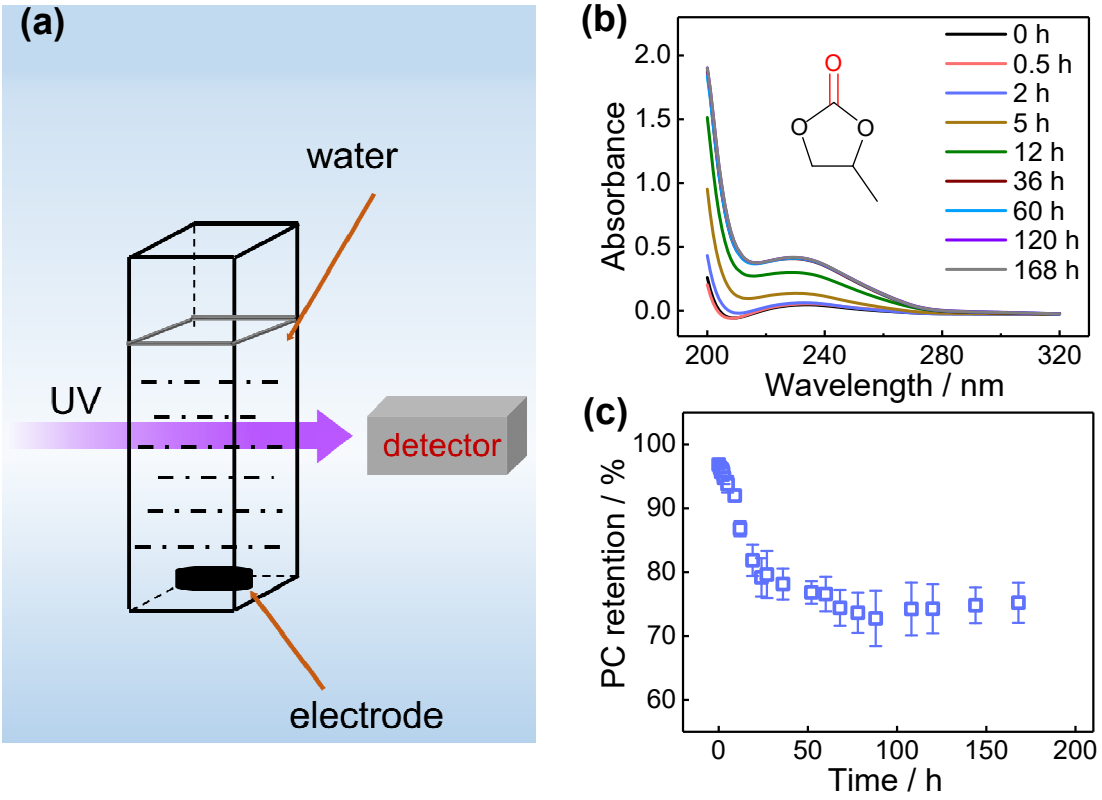

Fig. S13. (a) Schematic illustration of the detection of the release of PC molecules from the activated carbon electrode to water using a UV/visible spectrophotometer. (b) Time dependence of UV spectra for the measurement of the release of PC molecules from the activated carbon electrode to water. (c) Time dependence of retention of PC molecules within the activated carbon electrode in water.

Fig. S13a schematically illustrates the detection of the release of PC molecules from the activated carbon electrode to water using a UV/visible spectrophotometer. The activated carbon electrode is immersed in PC for 40 min, and then is taken out from PC and put into pure water. In Fig. S13b, the absorption peak at ~ 230 nm is due to the carbonyl group of PC. In Fig. S13c, the time dependence of PC retention is obtained on the basis of the results shown in Fig. S13b. The initial decrease in PC retention should be attributed to the diffusion of the free PC molecules from the pores of the activated carbon electrode to water.

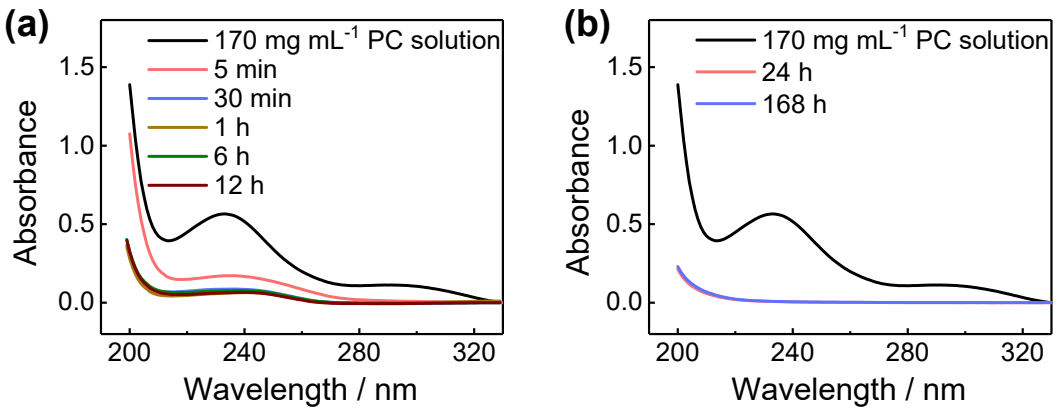

Fig. S14. (a) Time dependence of UV spectra of the aqueous solution during the adsorption of PC molecules from the bulk aqueous solution (170 mg mL^{-1}, 2.0 mL) to the activated carbon electrode (surface area of 13.6 cm^2, thickness of 200 μm). (b) Time dependence of UV spectra of the aqueous solution during the desorption of PC molecules from the activated carbon electrode to water after the adsorption equilibrium is reached in panel (a).

A bare activated carbon electrode is put into an aqueous PC solution to allow the PC molecules to be adsorbed on the surface of the activated carbon electrode (Fig. S14a). After the adsorption equilibrium is reached, the activated carbon electrode is taken out from the aqueous PC solution, and then is put into pure water. No obvious desorption of the PC molecules from the activated carbon electrode to water can be observed (Fig. S14b), further suggesting that the stably adsorbed interfacial PC layer can prevent the electrode from contacting water.

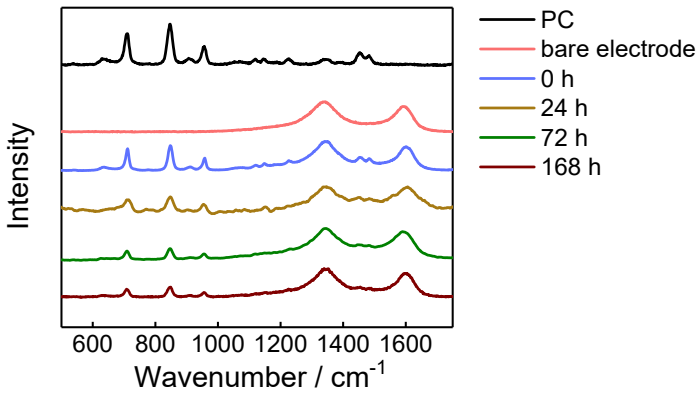

Fig. S15. Time dependence of Raman spectra of the activated carbon electrode during the desorption of PC molecules from the activated carbon electrode to water.

The activated carbon electrode is immersed in PC for 40 min, and then is taken out from PC and put into pure water for monitoring the release of PC molecules from the activated carbon electrode by measuring the Raman spectra of the activated carbon electrode with time. In Fig. S15, the peaks at ~ 710 cm^{-1}, ~ 849 cm^{-1}, and ~ 959 cm^{-1} arise from the PC molecules, and the peaks at ~ 1340 cm^{-1} and ~ 1600 cm^{-1} arise from the activated carbon electrode.

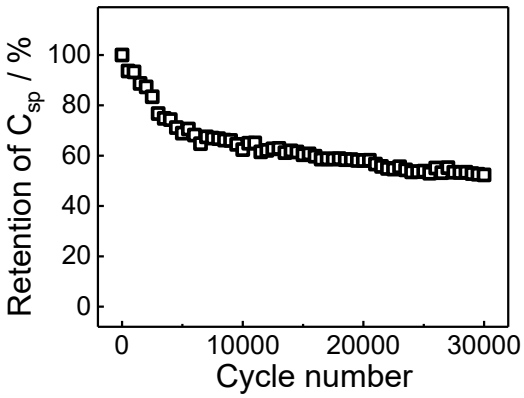

Fig. S16. Cycling performance of the PPDP-Li^+/Na^+-PC-based QSEDLC at a current density of 1.0 A g^{-1} with an EDW of 2.7 V.

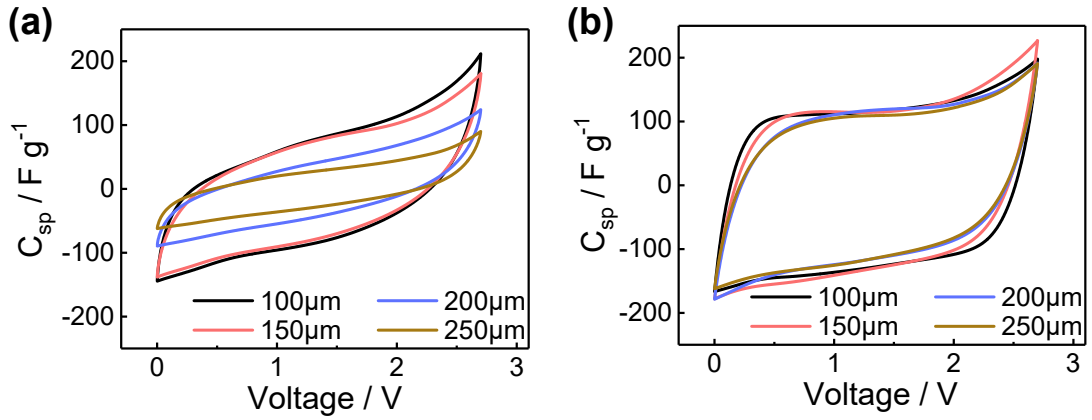

Fig. S17. CV curves of the supercapacitors with different electrode thicknesses at a scan rate of 100 mV s^{-1}. (a) PPDP-Li^+/Na^+-based QSEDLCs. (b) PPDP-Li^+/Na^+-PC-based QSEDLCs.

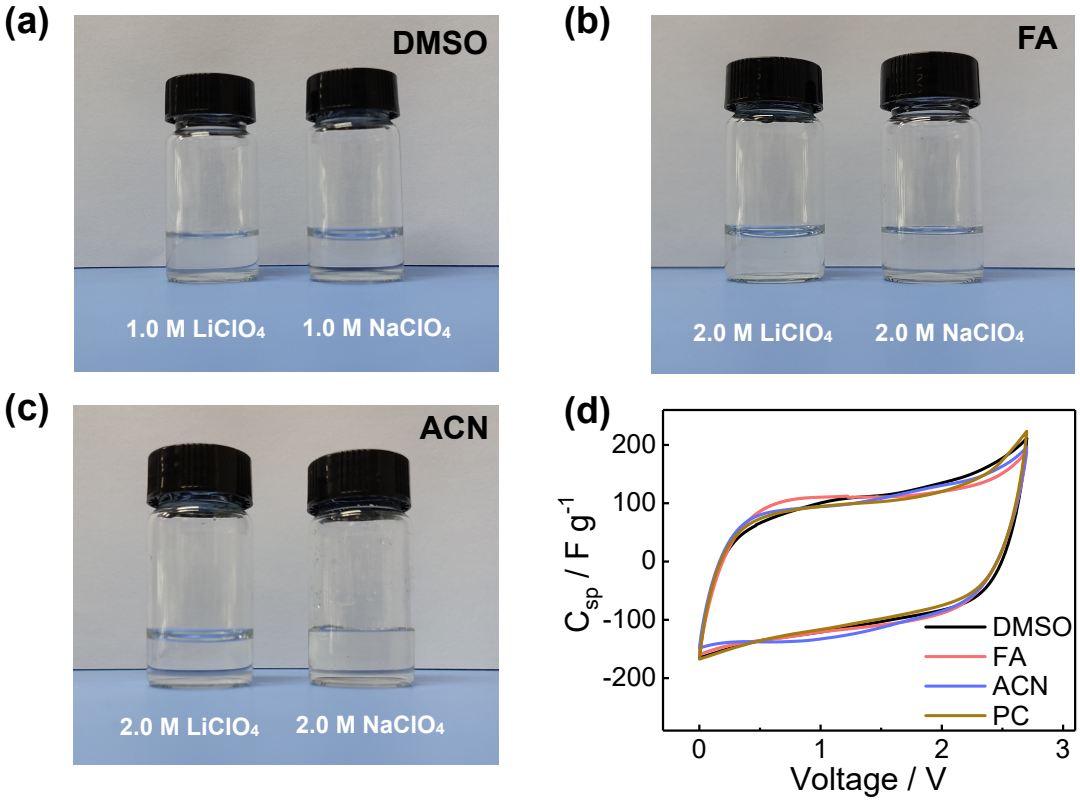

Fig. S18. (a) The image of the DMSO electrolyte solutions. (b) The image of the FA electrolyte solutions. (c) The image of the ACN electrolyte solutions. (d) CV curves for the PPDP-Li^+/Na^+-organic solvent-based supercapacitors at a scan rate of 100 mV s^{-1}.

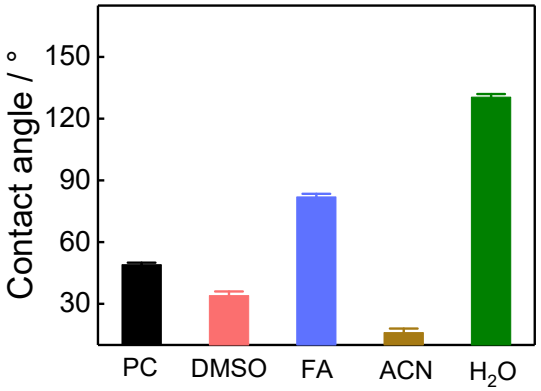

Fig. S19. Contact angles of PC, DMSO, FA, ACN, and H_2O on the surface of the activated carbon electrode at ~ 25 °C.

Fig. S19 shows that the contact angle of PC is larger than those of DMSO and ACN but is smaller than that of FA. Nevertheless, in comparison with water which has a contact angle of ~ 131° on the surface of the activated carbon electrode, the contact angles of all these organic solvents are less 90°, suggesting that these organic solvents have a better wettability on the surface of the activated carbon electrode than water.

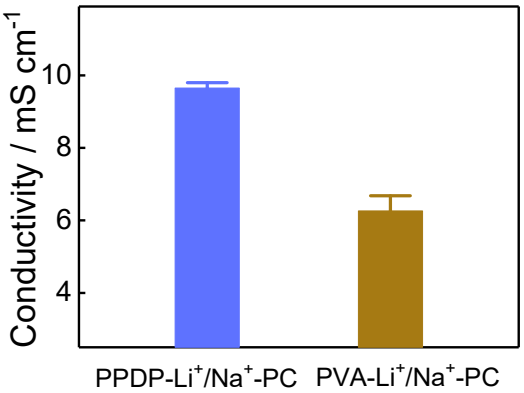

Fig. S20. The ionic conductivities of PPDP-Li^+/Na^+-PC and PVA-Li^+/Na^+-PC determined from the EIS measurements at ~ 25 °C.

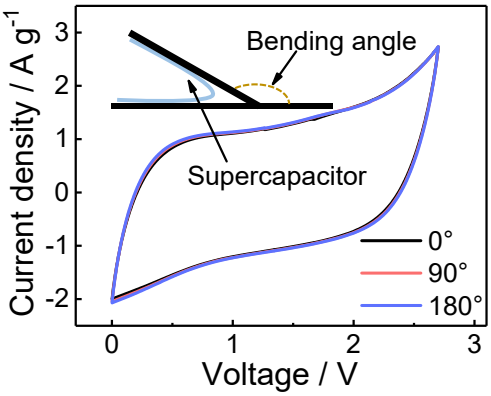

Fig. S21. CV curves for the PPDP-Li^+/Na^+-PC-based QSEDLC at different bending angles at a scan rate of 50 mV s^{-1} in the range of voltage from 0 to 2.7 V.

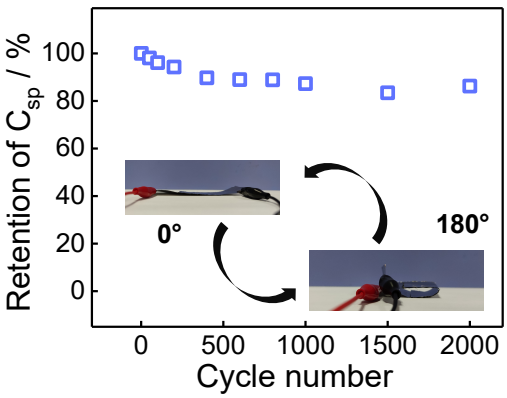

Fig. S22. Capacitance retention of the PPDP-Li^+/Na^+-PC-based QSEDLC as a function of cycle number for the repetitive bending between 0° and 180° with an operating voltage of 2.7 V.

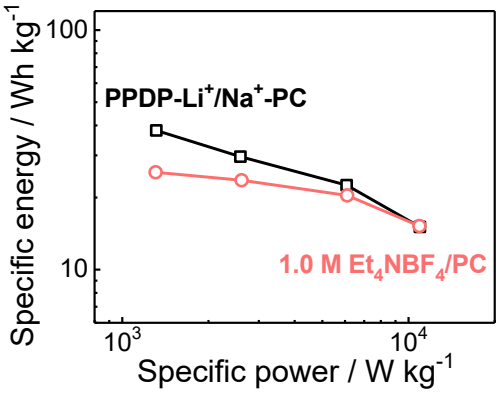

Fig. S23. Ragone plots of the PPDP-Li^+/Na^+-PC-based QSEDLC and the supercapacitor based on the commercial organic electrolyte (1.0 M tetraethylammonium tetrafluoroborate (Et_4NBF_4)/PC solution)[S1] with an EDW of 2.7 V employing the YP-50F activated carbon electrodes.

Table S1. Comparison between the PPDP-Li^+/Na^+-PC-based QSEDLC and the supercapacitor based on the commercial organic electrolyte (1.0 M Et_4NBF_4/PC solution).[S1]

	assembling condition	suitability for the wearable devices
PPDP-Li^+/Na^+-PC-based QSEDLC	in air	yes
1.0 M Et_4NBF_4/PC-based supercapacitor	in a water-free environment	no

References

S1 X. D. Bu, L. J. Su, Q. Y. Dou, S. L. Lei and X. B. Yan, *J. Mater. Chem. A*, 2019, **7**,7541-7547.

S2 Q. Y. Dou, L. Y. Liu, B. J. Yang, J. W. Lang, X. B. Yan, *Nat. Commun*. 2017, **8**, 2188.

S3 K. K. Ge and G. M. Liu, *Chem. Commun.*, 2019, **55**, 7167-7170.

S4 P. L. Taberna, P. Simon and J. F. Fauvarque, *J. Electrochem. Soc.*, 2003, **150**, A292.

S5 X. Yang, F. Zhang, L. Zhang, T. F. Zhang, Y. Huang and Y. S. Chen, *Adv. Funct. Mater.*, 2013, **23**, 3353-3360.